Research Article

Journal of Labelled Compounds and Radiopharmaceuticals

Received 29 September 2014, Revised 22 December 2014, Accepted 4 March 2015 Published online 19 April 2015 in Wiley Online Library

(wileyonlinelibrary.com) DOI: 10.1002/jlcr.3284

Development of a series of novel carbon-11 labeled PDE10A inhibitors

Vladimir Stepanov,[a]* Shotaro Miura,[a,b] Akihiro Takano,[a] Nahid Amini,[a] Ryuji Nakao,[a] Tomoaki Hasui,[b] Kosuke Nakashima,[b] Takahiko Taniguchi,[b] Haruhide Kimura,[b] Takanobu Kuroita,[b] and Christer Halldin[a]

Phosphodiesterase 10A (PDE10A) is a member of the PDE family of enzymes that degrades cyclic adenosine monophosphate (cAMP) and cyclic guanosine monophosphate (cGMP). Our aim was to label a series of structurally related PDE10A inhibitors with carbon-11 and evaluate them as potential positron emission tomography (PET) radioligands for PDE10A using nonhuman primates. The series consisted of seven compounds based on the 3-(1*H*-pyrazol-5-yl)pyridazin-4(1*H*)-one backbone. These compounds were selected from the initial larger library based on a number of parameters such as affinity, selectivity for hPDE10A in *in vitro* tests, lipophilicity, and on the results of multidrug resistance protein 1 (MDR1)-LLCPK1 and the parallel artificial membrane permeability assays. Seven radioligands (KIT-1, 3, 5, 6, 7, 9, and 12) were radiolabeled with carbon-11 employing O-methylation on the hydroxyl moiety using [^{11}C]methyl triflate. In vivo examination of each radioligand was performed using PET in rhesus monkeys; analysis of radiometabolites in plasma also was conducted using HPLC. All seven radioligands were labeled with high (>90%) incorporation of [^{11}C]methyl triflate into their appropriate precursors and with high specific radioactivity. Carbon-11 labeled KIT-5 and KIT-6 showed high accumulation in the striatum, consistent with the known anatomical distribution of PDE10A in brain, accompanied by fast washout and high specific binding ratio. In particular [^{11}C]KIT-6, named [^{11}C]T-773, is a promising PET tool for further examination of PDE10A in human brain.

Keywords: phosphodiesterase; PDE10A; carbon-11; PET; positron emission tomography; nonhuman primate

Introduction

Phosphodiesterase 10A (PDE10A) is a dual-substrate enzyme belonging to the phosphodisterase group that can hydrolyze adenosine and guanosine monophosphates (cAMP and cGMP). Both cAMP and cGMP are important intracellular signaling molecules activating numerous signaling pathways by interacting with kinases, receptors, and ion channels.[1] PDE10A is selectively expressed within medium spiny neurons of the striatum and in substantia nigra in the mammalian brain.[2] The localization, coupled with the regulatory function, of PDE10A in neurons and low levels of PDE10A expression in other areas of the brain has led to the hypothesis that inhibiting PDE10A might be a promising therapeutic approach for treating major CNS pathologies such as schizophrenia and attention deficit hyperactivity disorder.[3,4] The inhibition of PDE10A results in an increase in cAMP levels, an effect that alternatively can be produced by inhibition of D2 receptors or by activation of D1 receptors; however, the direct inhibition of PDE10A might reduce some of the undesirable side effects of dopamine receptor-targeted drugs.[5,6] Based on this information, PDE10A could conceivably be a drug target for several CNS disorders. The development of drugs targeting PDE10A is, however, hampered by the lack of suitable positron emission tomography (PET) radioligands specific for this enzyme. As an imaging technique and translational tool, PET would allow *in vivo* quantification of PDE10A levels, providing information regarding target occupancy by potential drugs, distribution and density of PDE10A in tissues, and the specificity of the drug molecule and tissue disposition.[7,8] In recent years, several molecules, such as [^{11}C]papaverine, [^{11}C]MP-10, [^{18}F]MNI659, and [^{18}F]JNJ41510417, have been proposed as potential PET radioligands for PDE10A.[9–13] However, to date, only one radioligand, [^{18}F]JNJ42259152, has been fully validated.[14,15] Additionally, current PDE10A radioligands may have some limitations, such as formation of lipophilic radiometabolites or less than optimal kinetics.[16–18] Thus, there is the need for validated PDE10A PET tracers with improved metabolic and/or kinetic profiles.

For the purposes of developing a radioligand suitable for clinical PET evaluation of PDE10A inhibitors, we labeled seven novel molecules from the drug portfolio of Takeda Pharmaceutical Company Ltd. (Japan) and evaluated their binding properties in a nonhuman primate (NHP) model. The series consisted of seven compounds based on the 3-(1*H*-pyrazol-5-yl)pyridazin-4(1*H*)-one backbone.[19] The compounds were selected from the initial library

[a]*Department of Clinical Neuroscience, Center for Psychiatric Research, Karolinska Institutet, Stockholm, Sweden*

[b]*CNS Drug Discovery Unit, Pharmaceutical Research Division, TAKEDA Pharmaceutical Company, Ltd., Fujisawa, Japan*

**Correspondence to: Vladimir Stepanov, Department of Clinical Neuroscience, Center for Psychiatric Research, Karolinska Institutet, Stockholm, Sweden. E-mail: vladimir.stepanov@ki.se*

of 26 compounds, and a final selection of seven was made based on parameters such as affinity (IC_{50} <5 nM, with exception of KIT-1), selectivity for hPDE10A in *in vitro* tests, lipophilicity (logP <3.0), and the results of the multidrug resistance protein 1 (MDR1)-LLCPK1 (MDR1–LLCPK1 score below 2) and parallel artificial membrane permeability assays (Table 1)[20,21]

The aim of this study was to develop a PDE10A radioligand with suitable characteristics for examination of PDE10A drug occupancy studies in a clinical setting.

Experimental

Reagents and instrumentation

Seven precursors for labeling and seven unlabeled reference standards were supplied by Takeda Pharmaceutical Company Ltd. (Japan).[19] All other chemicals were of analytical grade, were obtained from commercial sources, and were used as received. Solid-phase extraction cartridges (Oasis HLB 1cc) were obtained from Water Corp. (Milford, MA, USA), and Millex GV 0.22-μm sterile filters were purchased from Millipore (Ireland). Sterile phosphate buffered saline was purchased from APL (Sweden). Radioligand purification was performed on a semipreparative HPLC system that consisted of rheodyne-type injector, Ascentis RP-Amide reverse-phase column (250 × 10mm, 5 μm), a fixed wavelength absorbance detector set to 254 nm (Knauer, Germany) in series with a PIN-diode detector for radioactivity detection and a HPLC pump (Smartline 1000, Knauer, Germany). The radiochemical purity of labeled products was determined with reverse-phase HPLC on a system consisting of Merck-Hitachi L-7100 pump, Merck-Hitachi L-7400 ultraviolet (UV) detector (set to 220 nm), D-7000 interface (Merck-Hitachi), a β-flow radiodetector (Beckman) for radioactivity detection, and an Ascentis RP-Amide reverse-phase HPLC column (150 × 4.6 mm, 3 μm, Sigma-Aldrich). Identification of the carbon-11 labeled compounds was made by coinjecting it with a known unlabeled standard of the compound and comparing the retention time between the UV and radioactive channels on the same HPLC system as for radiochemical purity determination. The specific radioactivity (SA) of labeled compounds was determined using a HPLC system consisting of Ascentis RP-Amide reverse-phase HPLC column (150 × 4.6 mm, 3 μm or 50 × 4.6 mm, 2.7 μm, Sigma-Aldrich) and Hewlett-Packard Series 1100 HPLC system composed of an autoinjector, variable-length UV detector, pump, and degasser. The radiometabolism of each labeled compound in NHPs was assessed using plasma samples analyzed on an HPLC system consisting of an injector (Rheodyne 7125), a Merck-Hitachi L-7100 pump, a Merck-Hitachi L-7400 UV detector (set to 254 nm) in series with a 150TR radiodetector (Packard Radiomatic), a Merck-Hitachi D-7000 interface, a β-flow radiodetector (Beckman) for radioactivity detection, and a μ-Bondapak C18 HPLC column (300 × 7.8 mm, 10 μm, Waters).

The carbon-11 labeled compound-containing fraction from the semipreparative HPLC was collected into a vial containing 50 ml of sterile water and 70–100 mg of sodium ascorbate. The resulting solution was then pushed through the Oasis HLB 1cc cartridge, previously conditioned by 5 ml of 99.4% ethanol and 5 ml of sterile water (in that order). After trapping the product, the cartridge was rinsed with 8 ml of sterile water; the product was then eluted with 1 ml of 99.4% ethanol and collected into sterile vial prefilled with 9–10 ml of phosphate-buffered saline. Finally, the product was passed through a 0.22-μm sterile filter (Millipore) in a particle-free aseptic environment.

Radiochemistry

[^{11}C]Methyl triflate

[^{11}C]Methane was produced via the $^{14}N(p,\alpha)^{11}C$ reaction using N_2–H_2 gas target, with 16.4 MeV protons on General Electric Medical Systems PET Trace cyclotron, with target beam current set to 35 μA and irradiation time from 15 to 25 min. [^{11}C]Methyl iodide was produced according to previously published methods.[22] In short, [^{11}C]methane from target was collected on a HaySep® trap cooled with liquid nitrogen and then released into the recirculation system where it was reacted with iodine vapor at 720°C. The reaction mixture containing [^{11}C]methane and [^{11}C]methyl iodide was recirculated for 5 min through HaySep® trap cooled to −20°C to trap the [^{11}C]CH_3I produced. To prepare [^{11}C]methyl triflate, the [^{11}C]methyl iodide was released from HaySep™ trap and swept through a heated quartz glass column containing silver-triflate impregnated graphitized carbon, as described elsewhere.[23]

General labeling procedure with [^{11}C]Methyl triflate

[^{11}C]Methyl triflate was trapped at room temperature in a glass reaction vial containing corresponding desmethylated precursor (0.2–0.4 mg), acetone (400–600 μl), and sodium hydroxide (0.5 M, 3 μl). [^{11}C]Methyl triflate was reacted with the precursor at room temperature for 60 s. The corresponding labeled product was purified using a reversed-phase HPLC, as described above. The total synthesis time was 35–40 min. The radiochemical purity analysis and identification was performed on an analytical HPLC system described above. The mobile phase composition for purification and analysis together with yield, radiochemical purity, and specific activity are summarized below.

1-(2-fluorophenyl)-5-[^{11}C]methoxy-3-(1-phenyl-1H-pyrazol-5-yl) pyridazin-4(1H)-one ([^{11}C]KIT-1) (Figure 1)

[^{11}C]KIT-1 was synthesized from 1-(2-fluorophenyl)-5-hydroxy-3-(1-phenyl-1H-pyrazol-5-yl)pyridazin-4(1H)-one and purified using acetonitrile/aq. triethylamine 0.1% 430:570 *v/v* as mobile phase at a flow of 6 ml/min. Radioactivity yield was 3675 ± 485 MBq, and radiochemical purity was >99.8%. The analysis was performed using acetonitrile/aq. phosphoric acid 0.05 M 450:550 *v/v*. Specific radioactivity was 455 ± 256 GBq/μmol (n = 2).

Table 1. Physicochemical and pharmacological properties of the seven compounds investigated in this report

Compound	IC50 (nM)	Selectivity for hPDE10A	Log D	MDR1-LLCPK1 score	PAMPA
KIT-1	12	780	1.75	0.7	257
KIT-3	0.49	5100	2.25	1.8	ND
KIT-5	4.7	13000	2.29	0.5	188
KIT-6	0.77	2900	2.13	0.6	233
KIT-7	0.38	6300	1.81	1.2	93
KIT-9	0.27	8900	1.39	2	132
KIT-12	2.1	6200	2.06	1	276

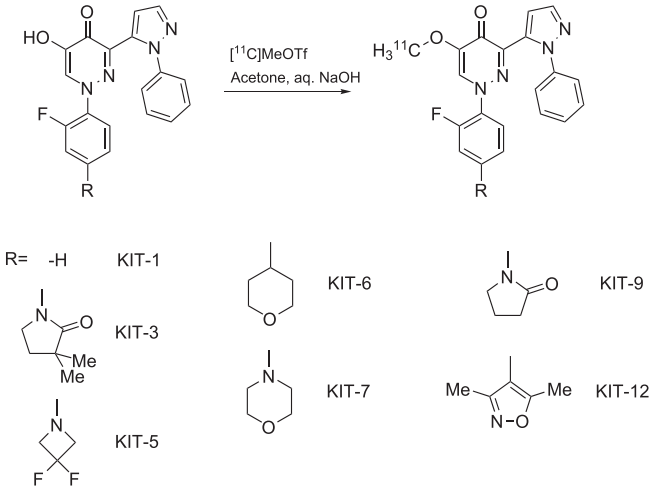

Figure 1. Summary of labeling procedure for [^{11}C]KIT-1, [^{11}C]KIT-3, [^{11}C]KIT-5, [^{11}C]KIT-6, [^{11}C]KIT-7, [^{11}C]KIT-9, and [^{11}C]KIT-12.

1-(4-(3,3-dimethyl-2-oxopyrrolidin-1-yl)-2-fluorophenyl)-5-[^{11}C]methoxy-3-(1-phenyl-1H-pyrazol-5-yl)pyridazin-4(1H)-one ([^{11}C]KIT-3) (Figure 1)

[^{11}C]KIT-3 was synthesized from 1-(4-(3,3-dimethyl-2-oxopyrrolidin-1-yl)-2-fluorophenyl)-5-hydroxy-3-(1-phenyl-1H-pyrazol-5-yl)pyridazin-4(1H)-one and purified using acetonitrile/aq. triethylamine 0.1% 470:530 *v/v* as mobile phase at a flow of 6 ml/min. Radioactivity yield was 3170 ± 300 MBq, and radiochemical purity >99%. The analysis was performed using acetonitrile/aq. phosphoric acid 0.05 M 500:500 *v/v*. Specific radioactivity was 517 ± 42 GBq/μmol ($n = 2$).

1-(4-(3,3-difluoroazetidin-1-yl)-2-fluorophenyl)-5-[^{11}C]methoxy-3-(1-phenyl-1H-pyrazol-5-yl)pyridazin-4(1H)-one ([^{11}C]KIT-5) (Figure 1)

[^{11}C]KIT-5 was synthesized from 1-(4-(3,3-difluoroazetidin-1-yl)-2-fluorophenyl)-5-hydroxy-3-(1-phenyl-1H-pyrazol-5-yl)pyridazin-4(1H)-one and purified using acetonitrile/aq. triethylamine 0.1% 500:500 *v/v* as mobile phase at a flow of 6 ml/min. Radioactivity yield was 2960 ± 380 MBq, and radiochemical purity >99.8%. The analysis was performed using acetonitrile/aq. phosphoric acid 0.05 M 530:470 *v/v*. Specific radioactivity was 775±399 GBq/μmol (n=2).

1-(2-fluoro-4-(tetrahydro-2H-pyran-4-yl)phenyl)-5-[^{11}C]methoxy-3-(1-phenyl-1H-pyrazol-5-yl)pyridazin-4(1H)-one ([^{11}C]KIT-6) (Figure 1)

[^{11}C]KIT-6 was synthesized from 1-(2-fluoro-4-(tetrahydro-2H-pyran-4-yl) phenyl)-5-hydroxy-3-(1-phenyl-1H-pyrazol-5-yl)pyridazin-4(1H)-one and purified using acetonitrile/aq. triethylamine 0.1% 440:560 *v/v* as mobile phase at a flow of 6 ml/min. Radioactivity yield was 2828 ± 351 MBq and radiochemical purity >99.5%. The analysis was performed using acetonitrile/aq. phosphoric acid 0.05 M 460:540 *v/v*. Specific radioactivity was 1643 ± 377 GBq/μmol ($n = 6$).

1-(2-fluoro-4-morpholinophenyl)-5-[^{11}C]methoxy-3-(1-phenyl-1H-pyrazol-5-yl)pyridazin-4(1H)-one ([^{11}C]KIT-7) (Figure 1)

[^{11}C]KIT-7 was synthesized from 1-(2-fluoro-4-morpholinophenyl)-5-hydroxy-3-(1-phenyl-1H-pyrazol-5-yl)pyridazin-4(1H)-one and purified using acetonitrile/aq. triethylamine 0.1% 410:590 *v/v* as mobile phase at a flow of 6 ml/min. Radioactivity yield was 2585 ± 170 MBq and radiochemical purity >99.5%. The analysis was performed using acetonitrile/aq. phosphoric acid 0.05 M 400:600 *v/v*. Specific radioactivity was 106 ± 34 GBq/μmol ($n = 2$).

1-(2-fluoro-4-(2-oxopyrrolidin-1-yl)phenyl)-5-[^{11}C]methoxy-3-(1-phenyl-1H-pyrazol-5-yl)pyridazin-4(1H)-one ([^{11}C]KIT-9) (Figure 1)

[^{11}C]KIT-9 was synthesized from 1-(2-fluoro-4-(2-oxopyrrolidin-1-yl) phenyl)-5-hydroxy-3-(1-phenyl-1H-pyrazol-5-yl)pyridazin-4(1H)-one and purified using acetonitrile/aq. triethylamine 0.1% 370:630 *v/v* as mobile phase at a flow of 6 ml/min. Radioactivity yield was 2445 ± 645 MBq and radiochemical purity >99%. The analysis was performed using acetonitrile/aq. phosphoric acid 0.05 M 400:600 *v/v*. Specific radioactivity was 501 ± 121 GBq/μmol ($n = 2$).

1-(4-(3,5-dimethylisoxazol-4-yl)-2-fluorophenyl)-5-[^{11}C]methoxy-3-(1-phenyl-1H-pyrazol-5-yl)pyridazin-4(1H)-one ([^{11}C]KIT-12) (Figure 1)

[^{11}C]KIT-12 was synthesized from 1-(4-(3,5-dimethylisoxazol-4-yl)-2-fluorophenyl)-5-hydroxy-3-(1-phenyl-1H-pyrazol-5-yl)pyridazin-4(1H)-one and purified using acetonitrile/aq. triethylamine 0.1% 470:530 *v/v* as mobile phase at a flow of 6 ml/min. Radioactivity yield was 1613 ± 196 MBq and radiochemical purity >99%. The analysis was performed using acetonitrile/aq. phosphoric acid 0.05 M 450:550 *v/v*. Specific radioactivity was 375 ± 303 GBq/μmol ($n = 2$).

PET measurements in NHPs

A total of 14 PET measurements were performed with three female rhesus monkeys (*Macaca mulatta*), with each of the seven radioligands evaluated in two different monkeys. The monkeys were housed in the Astrid Fagraeus Laboratory of the Swedish Institue for Infectious Disease Control, Solna, Sweden. The study was approved by the Animal Ethics Committee of the Swedish Animal Welfare Agency and was performed according to 'Guidelines for planning, conducting and documentic experimental research' (Dnr 4820706-600) of the Karolinska Institutet and international guidelines.[24] Anesthesia of the monkeys was induced by intramuscular injection of ketamine hydrochloride (~10 mg/kg, Ketaminol vet.; Intervet, Sollentuna, Sweden) and maintained by the administration of a mixture of sevoflurane (2–8%, Sevoflurane®; Abbott Scandinavia AB, Solna, Sweden), oxygen, and medical air after endotracheal intubation. The head was immobilized with a fixation device.[25] Body temperature was maintained by a Bair Hugger device (model 505; Arizant Health Care, MN, USA) and monitored by an oral thermometer. Electrocardiogram, heart rate, respiratory rate, oxygen saturation, and arterial blood pressure were continuously monitored throughout the experiment. PET measurements were conducted using the High Resolution Research Tomograph system (Siemens Molecular Imaging, TN, USA). A six-minute transmission scan using a single ^{137}Cs source was obtained immediately before the radioligand injection. List-mode data were acquired for 123 min. PET images were reconstructed with a series of frames of increasing duration (9 × 20, 3 × 60, 5 × 180, and 17 × 360 s) using the ordinary Poisson three-dimensional ordered-subset expectation maximization algorithm, with 10 iterations and 16 subsets, including modeling of the point spread function, after correction for attenuation, random, and scatter. The in-plane resolution of the reconstructed images was approximately 1.5 mm.[26]

Venous blood sampling (1–2 ml each) was performed at −5 min (for protein binding) and 4, 15, 30, 60, 90, and 120 min (for radiometabolite analysis) after the radioligand injection.

Regions of interest (ROI) for the whole brain was delineated manually on the coregistered magnetic resonance imaging (MRI)/PET images for all seven PET radioligands. The time activity curves of the ROIs were generated by applying the ROI to the dynamic PET data. The data were expressed as % injected dose (%ID), which is the total uptake (MBq) in the region divided by the injected radioactivity (MBq) × 100.

For the evaluation of regional brain uptake, the ROIs were delineated manually on the putamen, caudate, frontal cortex, temporal cortex, and cerebellum on the coregistered MRI images. The time radioactivity curves of the ROIs were generated by applying the ROI to the dynamic PET data. The data were expressed as % standard uptake value (%SUV), which is regional uptake (MBq/cc)/injected radioactivity (MBq) × body weight (g) × 100.

Radiometabolite and protein binding measurements

A reversed-phase HPLC method was used to determine the percentages of radioactivity in monkey plasma that corresponded to unchanged radioligand and radiometabolites during the course of the PET measurements. The plasma (0.5–1.5 ml), obtained after centrifugation of blood (1–3 ml) at 4000 g for 4 min, was mixed with 1.4 times volume of acetonitrile. After stirring with a vortex mixer, the sample was centrifuged at 4000 g for 4 min and was then analyzed by gradient HPLC using the following conditions: column; μ-Bondapak-C18 (300 × 7.8 mm, 10 μm; Waters), mobile phase; acetonitrile/0.1 M aq. ammonium formate, gradient from 30:70 to 70:30, 0–6 min, 70:30, 6–8 min, flow rate; 6.0 ml/min. Radioactivity in the blood (1.0–3.0 ml) and plasma (0.5–1.5 ml) was counted in a NaI well counter. The radioactivity of the protein precipitate fraction was also measured to quantify the recovery after precipitation with acetonitrile. Peaks for radioactive compounds eluting from the column were integrated, and their areas expressed as a percentage of the sum of the areas of all detected radioactive compounds (decay corrected to the time of injection on the HPLC).

An ultra-filtration method was used to estimate the free fraction of each of the seven PET radioligands in monkey plasma. Monkey plasma (500 μl) or a phosphate buffered saline solution (pH 7.4) (500 μl) as a control was mixed with each PET radioligand solution (50 μl, approximately 1 MBq) and incubated at room temperature for 10 min. After the incubation, 200 μl portions of the incubation mixtures were pipetted into ultrafiltration tubes (Centrifree YM-30; Millipore) and centrifuged at 1500 g for 15 min. Equal aliquots (20 μl) of the ultrafiltrate and of the plasma were counted with a NaI well counter. The results were corrected for filter membrane binding as measured with the control samples.

Results and discussion

Radiochemistry

In-target produced [^{11}C]methane allowed for production of [^{11}C]methyl triflate, which was used for preparation of all seven PET radioligands with a high specific radioactivity of 624 ± 219 GBq/μmol (range of 72–2020 GBq/μmol, $n = 18$) at the time of radioligand administration, thus ensuring radioligand dose conditions in the PET measurements for all seven radioligands. The labeling chemistry for all radioligands was based on methylation of the hydroxyl group using [^{11}C]methyl triflate in acetone in the presence of a strong base (NaOH). The incorporation of [^{11}C]methyl triflate into the precursor was high (>90%) for all seven PET radioligands with a mean decay-corrected total radiochemical yield of 72% ($n = 15$, range of 60–90%).

PET measurements in NHPs

The mean ± SD-administered radioactivity for each injection into the rhesus monkey was 156 ± 2 MBq, corresponding to the injected mass of carrier ranging from 0.06 to 1.02 μg. The summation images of brain radioactivity show high and heterogeneous uptake of [^{11}C]KIT-5 and [^{11}C]KIT-6 and [^{11}C]KIT-7 (Figure 2).

The other compounds—[^{11}C]KIT-1, [^{11}C]KIT-3, [^{11}C]KIT-9, and [^{11}C]KIT-12—showed lower brain uptake. Between [^{11}C]KIT-5, [^{11}C]KIT-6, and [^{11}C]KIT-7, the summed radioactivity for [^{11}C]KIT-6 was the lowest due to a faster washout. The visual indications of high levels of whole brain uptake of [^{11}C]KIT-5 and [^{11}C]KIT-7 might indicate higher nonspecific binding and/or slower elimination of these compounds. The high uptake and fast washout of [^{11}C]KIT-1 might be explained by the relatively low binding affinity of this ligand to hPDE10A (12 nM) and faster metabolism compared to other radioligands, as described later.

Time-activity curves for whole brain uptake (Figure 3) are in agreement with visual indications from summation images (Figure 2).

After intravenous administration to rhesus monkey, the maximum mean ± SD brain radioactivity for [^{11}C]KIT-6 was 3.7 ± 0.4 %ID and washout was fast, while [^{11}C]KIT-5 displayed higher maximum brain radioactivity (4.2 ± 0.9 %ID) and slower washout. For [^{11}C]KIT-7, the maximum brain radioactivity was 2.4 ± 0.8 %ID, but washout was considerably slower compared with [^{11}C]KIT-5 and [^{11}C]KIT-6 due to higher binding affinity (0.38 nM; Table 1). Radioligand [^{11}C]KIT-1 exhibited a maximum whole brain radioactivity of 2.9 ± 0.5 %ID and very fast washout, followed by slow increase of radioactivity in the brain—a possible explanation for this is the formation of brain-

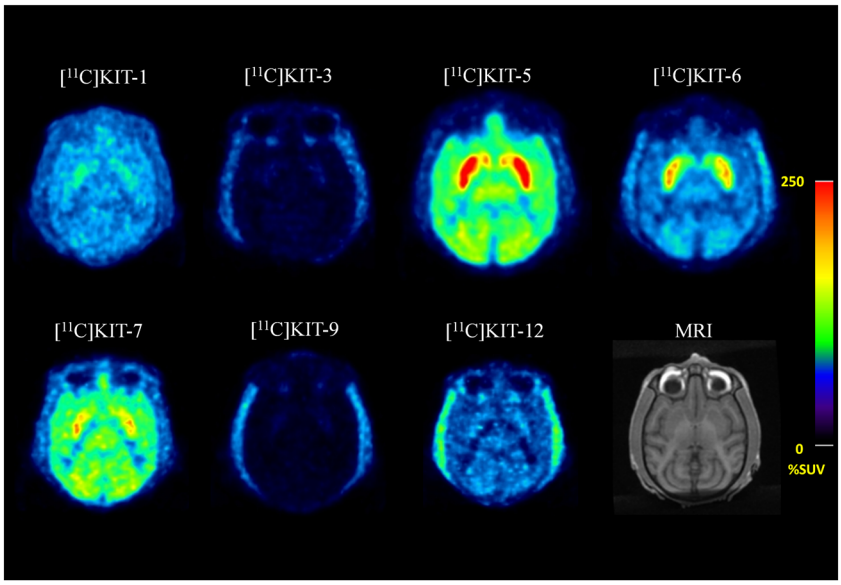

Figure 2. The representative summation images of the seven PET radioligands. The PET dynamic data of 9 min to 123 min were summed as summation images. The color scales were adjusted to the injected radioactivity.

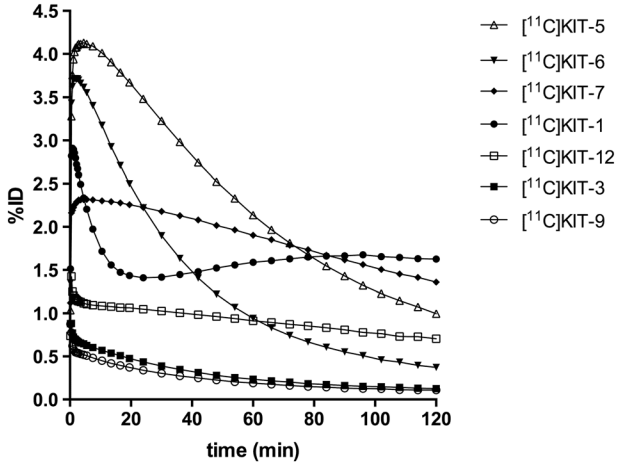

Figure 3. Whole brain uptake of the seven PET radioligands (%ID versus time (min)) The data is the average of two monkeys for each radioligand (variability between two experiments was between 1.2 and 1.8 %ID).

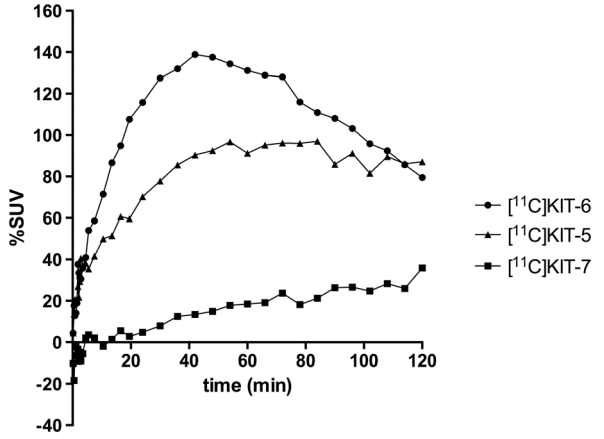

Figure 5. Specific binding of three PET radioligands (%SUV putamen minus cerebellum versus time (min)). The data is the average of two PET measurements for each radioligand.

penetrating radiometabolites. The whole brain uptake was negatively correlated with the results of the MDR1-LLCPK1 assay, with ligands scoring low in the assay having higher brain penetration because they are not P-glycoprotein (PGP) substrates. Ligands with MDR1-LLCPK1 assay scores above 1.5 displayed very poor whole brain uptake ([^{11}C]KIT-3 and [^{11}C]KIT-9, 1.8 and 2), possibly as a result of PGP-mediated efflux. A value of logD value <1.5 was associated with poor brain uptake as expected; [^{11}C]KIT-9, with a logD value of 1.39, displayed poor brain uptake. For the ligands displaying good whole brain uptake, the values of logD and MDR1-LLCPK1 assay scores are within optimal limits, that is between 1.5 and 3 for logD and below 1.5 for an MDR1-LLCPK1 assay score. In the whole brain uptake, three PET radioligands, [^{11}C]KIT-5, [^{11}C]KIT-6, and [^{11}C]KIT-7, showed acceptable kinetics for further evaluation.

Regional time-activity curves of the seven compounds are shown in Figure 4.

All radioligands, with the exception of [^{11}C]KIT-3 and [^{11}C]KIT-9, which exhibited very poor whole brain uptake, showed heterogeneous brain distribution, with the highest binding in the putamen and caudate and lowest binding in cortical regions. [^{11}C]KIT-5, [^{11}C]KIT-6, and to a relatively lower extent, [^{11}C]KIT-7, displayed heterogeneous distribution with a rank order consistent with the regional distribution of PDE10A *in vitro*.[27] The high level of nonspecific binding and slow washout (due to the high binding affinity) in case of

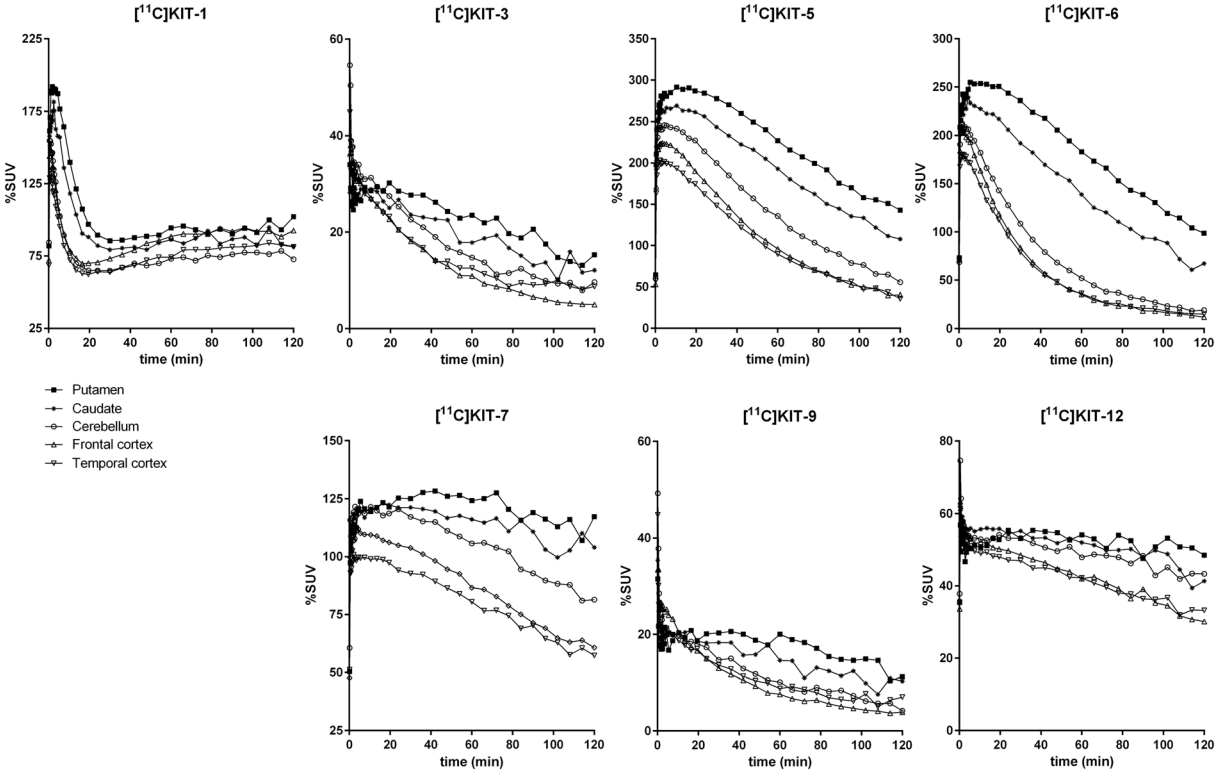

Figure 4. Regional brain uptake of three PET radioligands (%SUV versus time (min)). The data is the average of two PET measurements for each radioligand.

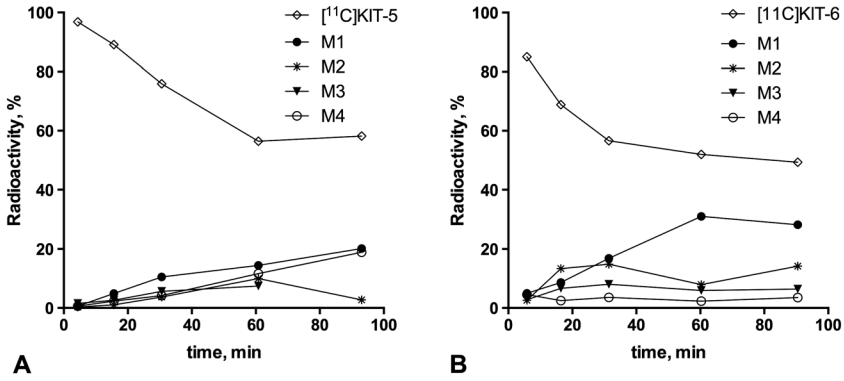

Figure 6. A – Time course of radiometabolism of [^{11}C]KIT-5. B – Time course of radiometabolism of [^{11}C]KIT-6.

[^{11}C]KIT-7 leads to a more homogenous binding throughout the brain.

Using cerebellum as a reference region for non-specific binding, time activity curves were generated for the specific binding of [^{11}C]KIT-5, [^{11}C]KIT-6, and [^{11}C]KIT-7 in the putamen, estimated as the difference in radioactivity in the putamen and cerebellum, shown in Figure 5.

The specific binding of [^{11}C]KIT-6 peaked at 40-min postinjection, reaching 140% of the SUV followed by a washout phase, whereas the specific binding of [^{11}C]KIT-5 peaked at approximately 90 %SUV at 50 minute postinjection without being followed by a clearly defined washout phase. [^{11}C]KIT-7 specific binding continued to increase throughout the experiment, suggesting a very slow off-rate of the ligand bound to the target, effectively making binding irreversible within experimental time frame. The specific binding ratio at 120 min between putamen and cerebellum was the highest for [^{11}C]KIT-6, 5.3 ± 0.9, followed by [^{11}C]KIT-5, 2.6 ± 0.1 and [^{11}C]KIT-7, 1.5 ± 0.2. The specific binding ratios of other ligands studied were at or below 1.5.

Thus, of the seven radioligands examined, three displayed significant binding heterogeneity and good brain penetration; of these three, [^{11}C]KIT-5 and [^{11}C]KIT-6 are considered to be the most promising due to the greater specific binding of these compounds in the putamen relative to [^{11}C]KIT-7.

Radiometabolite and protein binding measurements

The radiometabolism of all radioligands was examined in rhesus monkey plasma by HPLC using equipment and conditions described above. Radiometabolism for all ligands showed similar general trends in terms of radiometabolites formed and rates of metabolism, with the exception of [^{11}C]KIT-1, which showed considerably faster metabolism (15% of unchanged radioligand remaining at 60 min, decay corrected). [^{11}C]KIT-6 showed slightly faster metabolism compared to [^{11}C]KIT-5, with the amount of unchanged radioligand being 85 and 95% at 4 min and 50 and 60% at 60 min, respectively (decay-corrected). The [^{11}C]KIT-7 metabolic profile was generally similar to that of [^{11}C]KIT-5 and [^{11}C]KIT-6, being only being slightly faster 40% of unchanged radioligand (decay corrected) remaining at 60 min. The four radiometabolites observed for all ligands were less liphophilic than their parent compounds, based on order of elution from the HPLC column. Figure 6 shows unchanged radioligand and radiometabolite fraction percentages at various times during PET measurements for [^{11}C]KIT-5 and [^{11}C]KIT-6. The metabolite peaks were for convenience designated M1 to M4 in order of elution from the HPLC column for each ligand.

In monkey plasma, the free fractions of [^{11}C]KIT-5 and [^{11}C]KIT-6 were 31 ± 0.3 and 40 ± 2%, respectively.

The rate of radiometabolism might be one of the factors contributing to the faster washout of [^{11}C]KIT-6, as faster peripheral metabolism creates a higher concentration gradient across tissue compartments, resulting in faster washout of the radioligand from the brain.

Conclusions

Of the seven radioligands based on a 3-(1*H*-pyrazol-5-yl) pyridazin-4(1*H*)-one backbone, three radioligands—[^{11}C]KIT-5, [^{11}C]KIT-6, and [^{11}C]KIT-7—displayed significant brain accumulation and distribution indicative of binding to PDE10A. Out of these three, the most promising was [^{11}C]KIT-6, which displayed the highest specific binding ratio and fastest washout. No formation of lipophilic radiometabolites was observed in monkey plasma, suggesting that [^{11}C]KIT-6, subsequently named [^{11}C]T-773, may be a promising PET radioligand for the visualization and quantification of PDE10A levels in mammalian brain.

Acknowledgements

This study was sponsored by Takeda Pharmaceutical Company Limited (Osaka, Japan). The authors thank animal care nurse Gudrun Nylen and all members of the PET group at the Karolinska Institutet for their excellent assistance during this study.

Conflict of Interest

The authors did not report any conflict of interest.

References

[1] T. Chappie, J. Humphrey, F. Menniti, C. Schmidt, *Curr. Opin. Drug Discovery Dev.* **2009**, *12*, 458–467
[2] T. F. Seeger, B. Bartlett, T. M. Coskran, J. S. Culp, L. C. James, D. L. Krull, J. Lanfear, A. M. Ryan, C. J. Schmidt, C. A. Strick, A. H. Varghese, R. D. Williams, P. G. Wylie, F.S. Menniti. *Brain Res.* **2003**, *985*, 113–126
[3] T. A. Chappie, C. J. Helal, X. Hou, *J. Med. Chem.* **2012**, *55*, 7299–7331
[4] J. Kehler, J. Nielsen, *Curr. Pharm. Des.* **2011**, *17*, 137–150
[5] C. J. Schmidt, D. S. Chapin, J. Cianfrogna, M. L. Corman, M. Hajos, J. F. Harms, *J. Pharmacol. Exp.* **2008**, *325*, 681–690
[6] J. A. Siuciak, D. S. Chapin, J. F. Harms, L. A. Lebel, S. A. McCarthy, L. Chambers, A. Shrikhande, S. Wong, F. S. Menniti, C. J. Schmidt, *Neuropharmacology* **2006**, *51*, 386–396
[7] C. Halldin, B. Gulyas, L. Farde. *Curr. Pharm. Des.* **2001**, *7*, 1907–1929

[8] C. M. Lee, L. Farde, *Trends Pharmacol. Sci.* **2006**, *27*, 310–316
[9] Z. Tu, J. Xu, L. A. Jones, S. Li, R. H. Mach, *Nucl. Med. Biol.* **2010**, *37*, 509–516
[10] C. Plisson, C. Salinas, D. Weinzimmer, D. Labaree, S.-F. Lin, Y-S. Ding, S. Jacobsen, P. W. Smith, R. E. Carson, R. N. Gunn, E. A. Rabiner, *Nucl. Med. Biol.* **2011**, *38*, 875–884.
[11] O. Barret, D. Thomae, D. Alagille, H. Lee, C. Papin, R. Baldwin, D. Jennings, K. Marek, J. Seibyl, G. Tamagnan, *J. Nucl. Med.* **2012**, *53*, S1, 361.
[12] S. Celen, M. Koole, M. De Angelis, I. Sannen, S. K. Chitneni, J. Alkazar, S. Dedeurwaerdere, D. Moechars, M. Schmidt, A. Verbruggen, X. Langlois, K. Van Laere, J.-L. Andres, G. Bormans, *J. Nucl. Med.* **2010**, *51*, 1584–1591.
[13] O. Barret, D. Thomae, A. Tavares, D. Alagille, C. Papin, R. Waterhouse, T. McCarthy, D. Jennings, K. Marek, D. Russell, J. Seibyl, G. Tamagnan, *J Nuc Med. pubished online June 4,* **2014** Doi: 10.2967/jnumed.113.122895
[14] K. Van Laere, R. U. Ahmad, H. Hudyana, K. Dubois, M. E. Schmidt, S. Celen, G. Bormans, M. Koole. *J. Nucl. Med.* **2013**, *54*, 1285–1289.
[15] K. Van Laere, R. U. Ahmad, H. Hudyana, S. Celen, K. Dubois, M. E. Schmidt, G. Bormans, M. Koole. *Eur. J. Nucl. Med. Mol. Imaging* **2013**, *40*, 254–261.
[16] J. Fan, X. Zhang, J. Li, H. Jin, P.K. Padakanti, L. A. Jones, H. P. Flores, Y. Su, J. S. Perlmutter, Z. Tu. *Biorg Med Chem.* **2014**, *22*, 2648–2654.
[17] Z. Tu, J. Fan, S. Li, L. A. Jones, J. Cui, P. K. Padakanti, J. Xu, D. Zeng, K. I. Shogi, J. S. Perlmutter, R. H. Mach. *Bioorg. Med. Chem.* **2011**, *19*, 1666–1673.
[18] S. Celen, M. Koole, M. Ooms, M. De Angelis, I. Sannen, J. Cornelis, J. Alcazar, M. Schmidt, A. Verbruggen, X. Langlois, K. Van Laere, J. I. Andrés, G. Bormans, *Neroimage* **2013**, *82*, 13–22.
[19] T. Taniguchi, T. Hasui, S. Miura, V. Stepanov, A. Takano, C. Halldin, Radiolabeled compounds and their use as radioradioligands for quantitative imaging of phosphodiesterase (PDE10A) in mammals, Japan, **2013**, WO/2013/027845
[20] J. Kunitomo, M. Yoshikawa, M. Fushimi, A. Kawada, J. F. Quinn, H. Oki, H. Kokubo, M. Kondo, K. Nakashima, N. Kamiguchi, K. Suzuki, H. Kimura, T. Taniguchi, *J. Med. Chem.* **2014**, *57*, 6927–9643.
[21] T. Takeuchi, S. Yoshitomi, T. Higuchi, K. Ikemoto, S.-I. Niwa, T. Ebihara, M. Katoh, T. Yokoi, S. Asahi. Pharmaceutical Research. **2006**, *23*, 1460–1472.
[22] J. Andersson, P. Truong, C. Halldin. *Appl. Radiat. Isot.* **2009**, *67*, 106–110.
[23] K. Någren, C. Halldin, L. Müller, C. G. Swahn, P. Lehikoinen. *Nucl. Med. Biol.* **1995**, *22*, 965–79.
[24] J. D. Clark, G. F. Gebhart, J. C. Gonder, M. E. Keeling, D. F. Kohn. *Ilar J.* **1997**, *38*, 41–48.
[25] P. Karlsson, L. Farde, C. Halldin, C. G. Swahn, G. Sedvall, C. Foged, K. T. Hansen, *B. Skrumsager. Psychopharmacology.* **1993**, *113*, 149–156.
[26] A. Varrone, N. Sjöholm, L. Eriksson, B. Gulyás, C. Halldin, L. Farde, *Eur. J. Nucl. Med. Mol. Imaging* **2009**, *36*, 1639–1650.
[27] T. M. Coskran, D. Morton, F. S. Menniti, W. O. Adamowicz, R. J. Kleiman, A. M. Ryan, C. A. Strick, C. J. Schmidt, D. T. Stephenson, *J. Histochem. Cytochem.* **2006**, *54*, 1205–1213.